24th Australasian Fluid Mechanics Conference – AFMC2024
Canberra Australia
1-5 December 2024
DOI:10.5281/zenodo.14213308
Paper No: AFMC2024-010

Free-surface turbulence in hydraulic jump breaking roller at low inflow Froude number

Jiayue Hu[1*], and Hubert Chanson[1]

[1] School of Civil Engineering, University of Queensland, Brisbane QLD 4072, Australia

* Email: jiayue.hu@uq.net.au

Abstract

A hydraulic jump occurs when a high-velocity supercritical flow in an open channel transition suddenly to a subcritical flow. In this study, new experiments with low inflow Froude numbers ($2.1 < Fr_1 < 3.8$) were conducted in a large-size facility using ultrasonic displacement metres and digital cameras. The study provided details of free surface turbulent fluctuations in hydraulic jump with relatively large Renolds numbers ($1.36\times10^5 < Re < 2.46\times10^5$). A time series analysis of the water surface elevation of the roller and the fluctuations of hydraulic jump toe perimeter were conducted. The results characterised the dynamic and unsteady nature of breaking jump roller. The findings offer valuable insights for researchers and engineers to enhance their comprehension of the physical processes involved.

1. Introduction

Many conveyance structures including dam spillways are equipped with an energy dissipation structure at the downstream end to dissipate the kinetic energy of the water energy and protect the riverbed downstream (Novak et al. 2007, Chanson and Carvalho 2015). Most stilling basin designs are engineered to facilitate hydraulic jumps (Chow 1959, Henderson 1966, Peterka 1958, Hager 1992). A hydraulic jump occurs at the transition from a supercritical flow with relatively small depth and high velocity to a subcritical flow with relatively large depth and low velocity (Henderson 1966, Chanson 2004) (Figure 1A). Key features of hydraulic jumps include strong turbulence, spray and splashing, and air entrainment. The flow within a hydraulic jump is not stationary. It exhibits a series of quasi-periodic movements that vary in both duration and magnitude. In addition to small-scale fast turbulent fluctuations, and the advection of air bubbles, the hydraulic jump toe oscillates around its mean position, accompanied by fluctuations of the free surface above the roller (Mouaze et al. 2005, Shi et al. 2021).

While there have were many investigations of hydraulic jumps with large inflow Froude numbers, little attention was directed towards the free-surface turbulence of hydraulic jumps with low Froude numbers. Only a limited number of studies explored the physical processes involved in these hydraulic jumps with low inflow Froude number and high Reynold number. The present study aimed to investigate the physical characteristics of free-surface fluctuations within a hydraulic jump roller, with a focus on hydraulic jumps with inflow Froude numbers from 2.1 to 3.8.

2. Physical facility, instrumentation and processing

The experimental investigations were conducted in a horizontal rectangular flume located within the Advanced Engineering Building (AEB) at the University of Queensland (UQ). The flume featured a channel width of 0.50m, sidewalls of 0.45m in height, and a flume length of 3.2m. The sidewalls were constructed using glass, and the channel bed was composed of HDPE material (Figure 1B). At the upstream end, the flow conditions were controlled by a vertical sluice gate equipped with a rounded

edge (Figure 1A). At the downstream end, the flow was controlled by an adjustable overflow gate. This flume was previously utilised in experimental studies conducted by Wang and Chanson (2015). In Figure 1A, x represents the longitudinal coordinate, with x = 0 denoting the position at the upstream undershoot gate, x_1 is the location of roller toe, while y and z denote the transverse and vertical coordinates, respectively. The inflow water depth and outflow water depth is d_1 and d_2 respectively, while the inflow velocity and outflow velocity is V_1 and V_2 respectively. The roller length is L_r. The free-surface water elevations were measured with Acoustic Displacement Meters (ADMs) Microsonic^{TM} Mic+25, point gauges, sidewall rulers and digital cameras (Figure 1B). The average water depth was determined using sidewall rulers and point gauges. Side ruler reading was checked against point gauge data and Acoustic Displacement Meters reading on the channel centre line with a very small difference. The ADM and video recordings provided the data for time series analyses of the water depth in the hydraulic jump. The ADM data were simultaneously collected from 12 sensors (Figure 2) with a sampling frequency of 200 Hz per sensor for a duration of 720s.The sideview videos were recorded using a Fujifilm^{TM} X-T30 II digital camera, equipped with a XF 18-55MM F2.8-4 R LM OIS lens. The camera was installed beside the channel and recorded the hydraulic jump flow through the glass sidewall. The camera was able to record videos in full HD resolution of 1920×1080 pixels with a maximum frame rate of 60 fps.

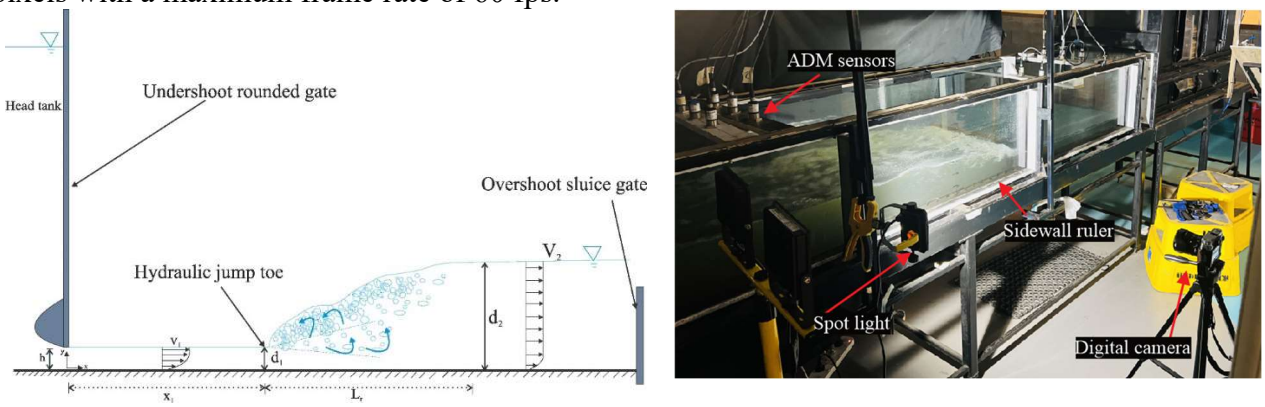

(A) (B)

Figure 1. Experimental facility – (A) Definition sketch of hydraulic jump; (B) Setup with sidewall ruler and digital camera (Flow condition: Fr_1=2.1, in this picture, the acoustic displacement meters are not correctly positioned due to issues with light reflection)

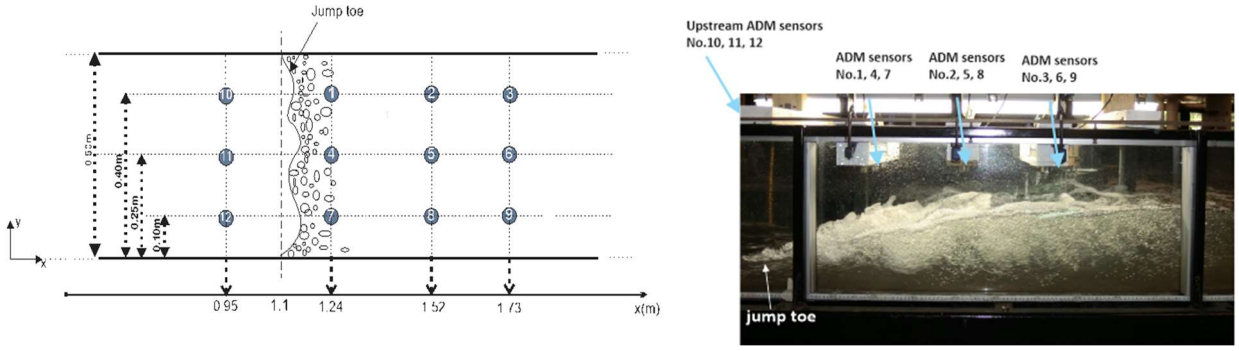

(A) (B)

Figure 2. Acoustic Displacement Meters (ADMs) experimental set up in the hydraulic jump flow – (A) Plan view of the 12 ADM sensors; (B) Side view for photograph of hydraulic jump and experimental setup (flow direction from left to right: x_1=1.1m, d_1=0.072m, Fr_1=2.6, Re=1.68×10^5)

3. Basic flow patterns

For all flow conditions, a breaking roller was observed, characterised by oscillatory patterns, significant air entrainment, spray, splashing and free-surface turbulence. Figure 3 illustrates some typical free-surface features of the air-water interface. The upstream supercritical flow impinged into the downstream subcritical flow area at the jump roller toe. The water level along of the roller presented a monotonic rise towards the corresponding conjugate depth. This was accompanied by some strong turbulence in both the free-surface region and within the turbulent roller. Downstream

of the roller, surface waves propagated and dispersed. The presence of large internal turbulent vortices was observed within the roller. A significant interaction between air and water was noted as part of the dynamics of the free surface. The large vortical structures and turbulent shear stress in the hydraulic jump's roller region were advected and broke up the entrapped air bubbles into smaller bubbles. The smaller air bubbles were moved into areas of lower shear stress, with an upward motion towards the recirculation region, resulting in some de-aeration. In the free-surface region near the jump toe, there were significant changes in the water surface level, along with energetic water splashing and the creation of foam due to the interaction between air and water. The existence of such air-water surface features was previously reported by Murzyn and Chanson (2009), Chanson (2011), Chachereau and Chanson (2011), Shi et al. (2021) in hydraulic jumps, across a range of Froude numbers. Details of the impingement region at the jump toe are shown in Figure 4.

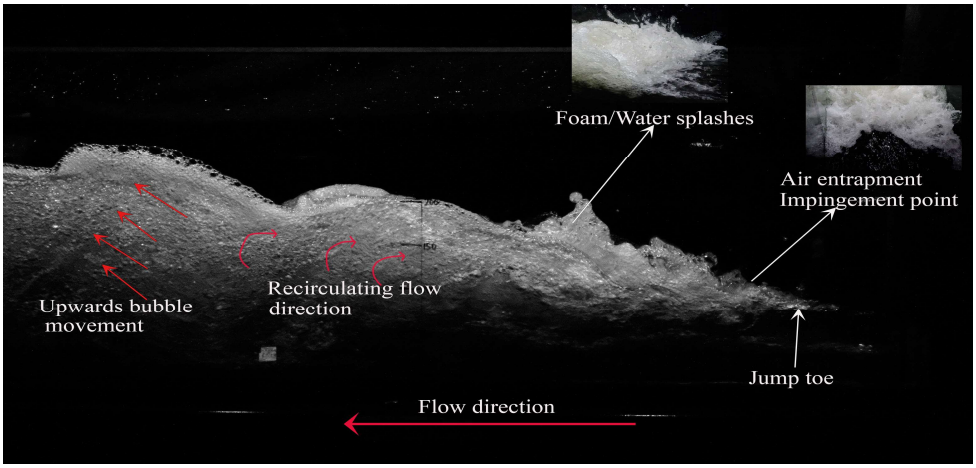

Figure 3. Aeration features in the hydraulic jump with Fr_1 = 3.1 and Re = 2.01×10^5, flow direction from right to left

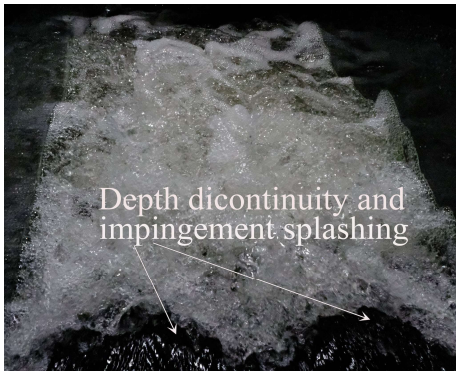

Figure 4. Details of the impingement edge at the jump toe. Looking downstream – Flow conditions: Q = 0.0883 m^3/s, d_1=0.07m, x_1=1.1m, Fr_1=3.045, Re=1.97×10^5 [Photo details: camera Fujifilm X-T30 II, shutter speed 1/500 s, 18mm focal length, f/20]

4. Free-surface characteristics

4.1 Hydraulic jump characteristics and free-surface profile

The water depth was directly obtained from the point gauge and sidewall ruler, although the data from ADM sensors were more detailed. The use of sidewall video further enhanced the extent of the data and the water surface fluctuations. Dimensionless longitudinal free-surface profiles are plotted in Figure 5A as a function of $\frac{x-x_1}{d_1}$, where x_1 is the location of the roller toe (x_1=1.1m), d is the median value of free-surface elevation above the channel bed, and x is longitudinal distance from the upstream gate. In Figure 5A & 5C, different colours show different inflow Froude numbers. All the longitudinal profiles were similar overall (Figure 5B).

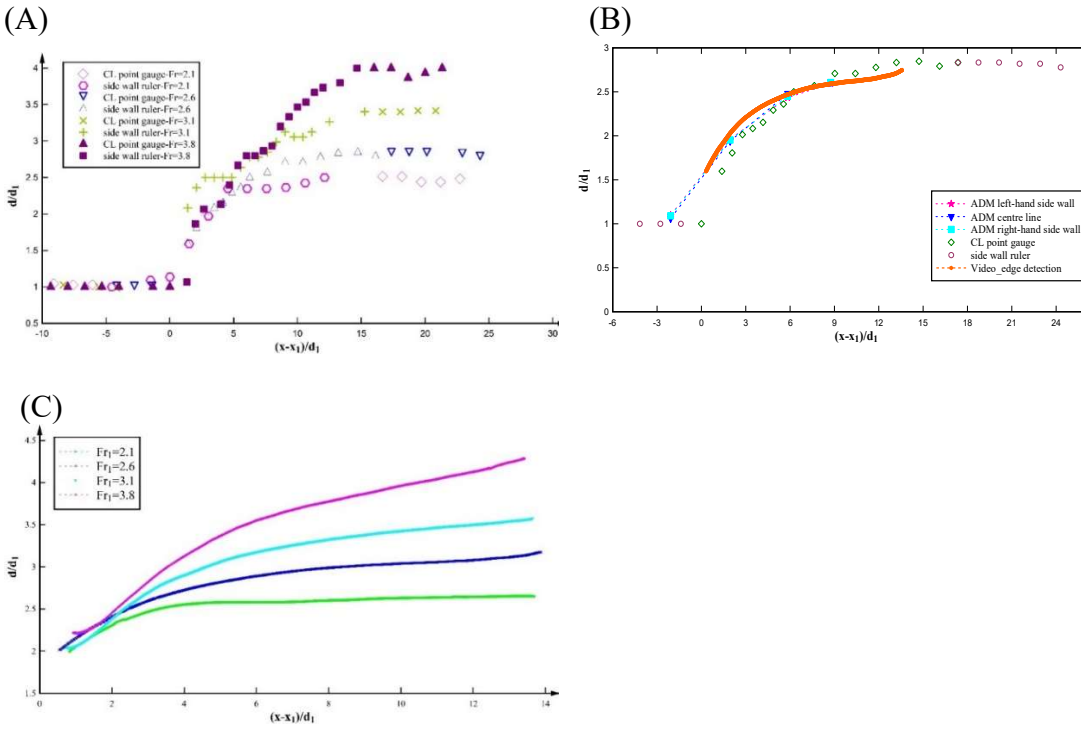

Figure 5. Dimensionless free surface profile – (A) Dimensionless median depth of free surface profile with point gauge and rular for Fr_1=2.1, 2.6, 3.1 and 3.8; (B) Dimensionless median depth of free surface profile with multiple sensors for Fr_1=2.6; (C) Dimensionless median depth of free surface profile with side view camera for Fr_1=2.1, 2.6, 3.1 and 3.8

The conjugate flow depth ratio d_2/d_1 is presented in Figure 6A as a function of the inflow Froude number Fr_1. The data compared with the equation of conservation of momentum, also called Bélanger equation:

$$\frac{d_2}{d_1} = \frac{1}{2} \times (\sqrt{1 + 8 \times {Fr_1}^2} - 1) \, . \qquad (1)$$

where d_1 and d_2 are respectively the upstream and downstream flow depths, Fr_1 is inflow Froud number.The roller length was observed to be L_r~0.45m for Fr_1=2.1, L_r~0.5m for Fr_1=2.31 and L_r~0.675m for Fr_1=2.6. The data followed closely the results of Wang and Chanson (2015) and Murzyn and Chanson (2009). More comparison are shown in Figure 6B. In summary, for the conjugate depth and roller length, the present data followed closely the established literature.

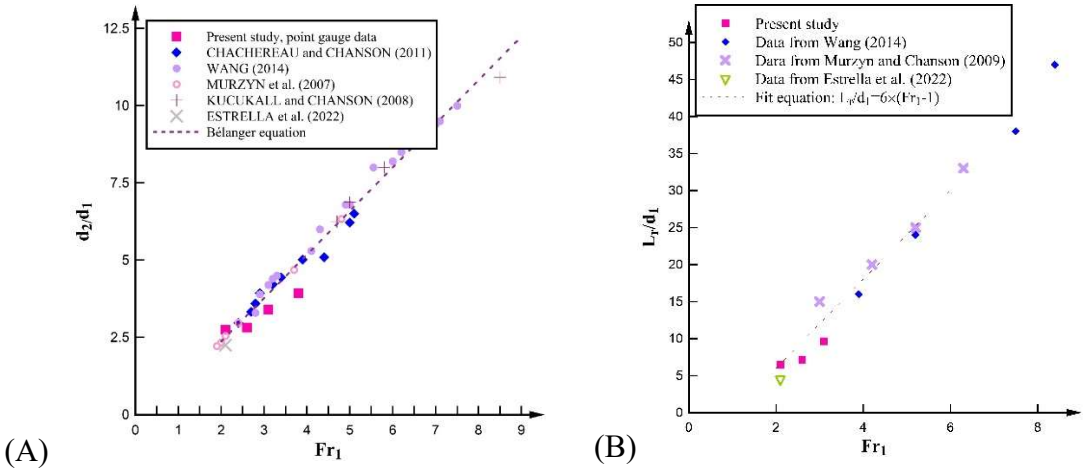

Figure 6. Conjugate depth ratio d_2/d_1 and dimensionless jump roller length Lr/d_1 as functions of inflow Froude number– Comparion with Bélanger equation, preivous experimental data- (A) Conjugate depth ratio (Point gauge data); (B) Dimensionless jump roller length and comparsion with other data sets

4.2 Free-surface fluctuations

The turbulent fluctuations of free surface elevation were quantified in terms of the quartile difference of water elevation (d_{75}-d_{25}), at various longitudinal positions for different inflow Froude numbers. In Figure 7, the ADM data (d_{75}-d_{25})/d_1 are plotted against the dimensionless distance from the jump toe (x-x_1)/d_1. The present data are centreline data recorded at four longitudinal locations. Some small free-surface fluctuations were observed upstream of the jump toe (x-x_1 < 0). A marked increase in free-surface fluctuations was seen immediately downstream of the jump toe (x-x_1 > 0) for all Froude numbers, and the free-surface fluctuations reached a maximum value $(d_{75}$-$d_{25})_{max}$ in the first half of the roller. The large free-surface fluctuations were associated with turbulence and linked to large vertical motions in the roller zone. Further downstream from the jump toe, the data presented a gradual reduction in free-surface fluctuations which increasing distance from the jump toe. The findings aligned with prior research by Mouaze et al. (2005), Kucukali and Chanson (2008), Murzyn and Chanson (2009) and Chacherau and Chanson (2011). The previous studies used all low inflow Froude number conditions but with relatively lower Reynolds number compared to present study.

A comparison between side and centre line ADM sensors data is shown in Figure 8. In the present study, the free-surface fluctuation, i.e. (d_{75}-d_{25})/d_1, was slightly lower on the channel centreline than near the sidewalls. This could be caused by the interaction between the flow and sidewalls, inducing three-dimensional eddies and increasing turbulence locally. These eddies can cause local variations in water depth, contributing to a higher quartile difference. The presence of eddies and increased turbulence disrupted the uniformity of the flow, causing localized differences in depth.

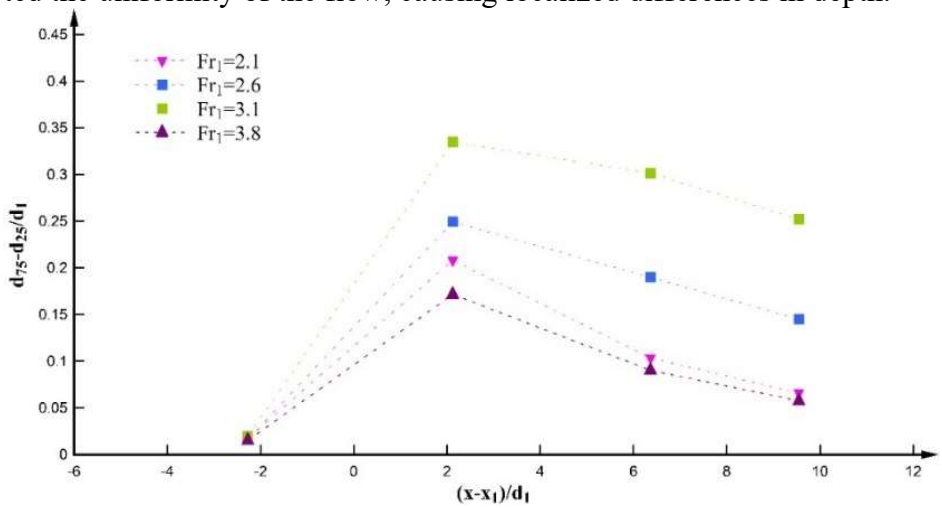

Figure 7. Dimensionless longitudinal profiles of free surface fluctuations d_{75}-d_{25}/d_1 in hydraulic jumps with multiple sensors;

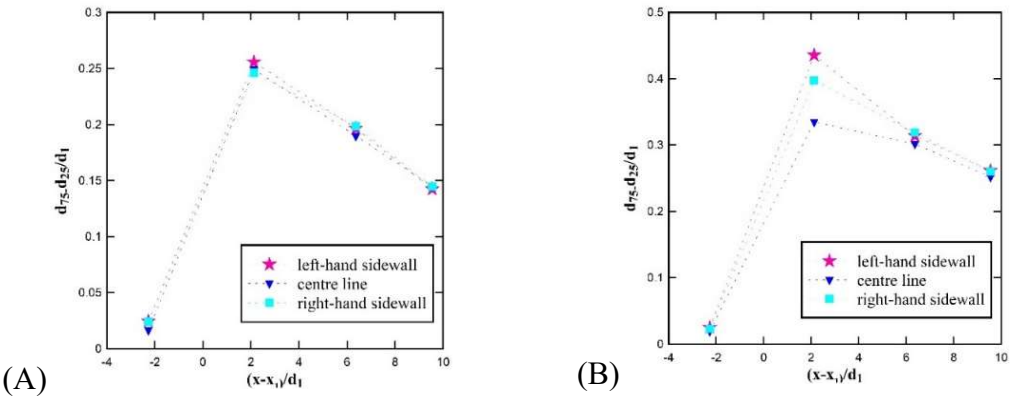

Figure 8. Comparison between centre line sensors and sidewall sensors on dimensionless longitudinal profiles of free surface fluctuations d_{75}-d_{25}/d_1 (A) Fr_1=2.6; (B) Fr_1=3.1

The free-surface vertical fluctuation analysis also derived from the sidewall camera, with a focus on the vertical velocity of the free-surface: $V_z = (\partial d/\partial t)_{z=d}$. The median value of the free-surface's vertical

velocity V_z is shown in Figure 9A. The data showed that V_z remained close to zero across all flow conditions as expected. While expected, this consistent median data outcome suggested that the hydraulic jump does not significantly perturb the free surface in the vertical direction, maintaining a steady flow profile regardless of the longitudinal position during the extended recording period. Figure 9B illustrates the variability in the free-surface vertical velocity, represented by V_{75}-V_{25} at different longitudinal positions for various flow conditions. The results showed that higher Froude numbers Fr_1 generally exhibited some increased velocity fluctuations, particularly around the jump roller. This variability highlighted the dynamic nature of the free surface under varying flow conditions, where increased turbulence and energy dissipation within the hydraulic jump led to more pronounced velocity fluctuations.

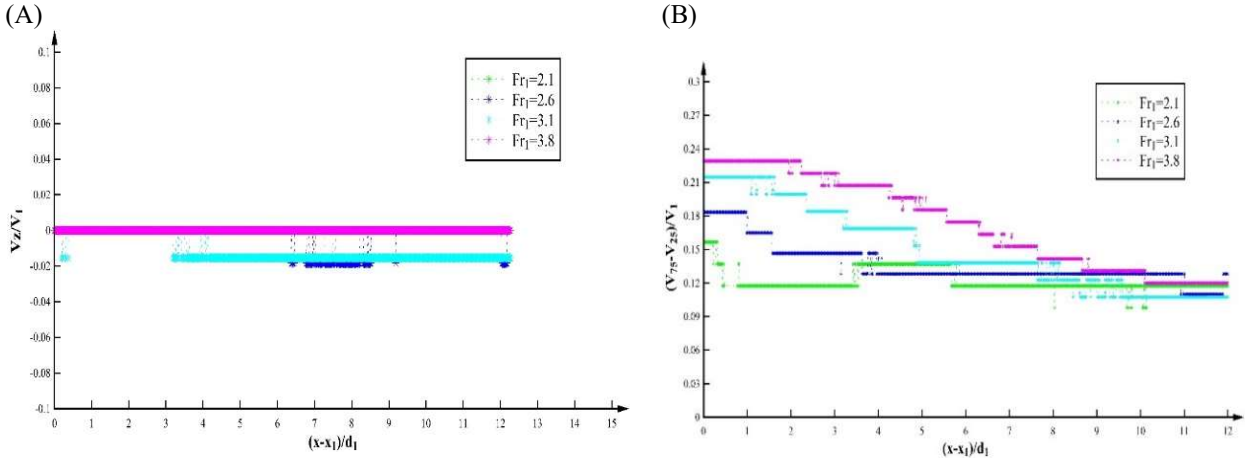

Figure 9. (A) Dimensionless free-surface vertical fluctuating velocity V_z in median value. (B) Dimensionless quartile difference of free-surface vertical fluctuating velocity V_{75}-V_{25}

4.3 Roller toe impingement perimeter

The longitudinal position of the hydraulic jump was observed to fluctuate around a mean position x_1, for all flow conditions. Previous studies (Long et al. 1991, Chanson and Gualtieri 2008, Murzyn and Chanson 2009) extensively studied the rapid oscillations of the jump toe position, albeit for large Froude numbers. The oscillations were believed to be associated with the formation of turbulent flow structures in the roller and air entrapment at the impingement point (Long et al. 1991). In the present analysis, the temporal median position of the roller toe impingement perimeter X_t, was computed at each transverse location, within the range $0 < y/W < 1$, where y is the transverse coordinate and W is the channel width. That is, X_t represents the temporal median at each distinct transverse location across the channel's width. The data were calculated over the duration of 200 s for each flow condition. Typical results are illustrated in Figure 10**,** presenting a cross-sectional view of the channel width for four Froude numbers. Figure 10 also includes 100 instantaneous transvers profiles for comparison. For all Froude numbers, the transverse profiles displayed a symmetrical pattern with a wavy shape. Among all flow conditions, the transverse wave length decreased as the Froude number increased. The current dataset revealed a slightly concave shape, suggestive of sidewall effects. The observation aligned with earlier findings by Shi et al. (2021), Zhang et al. (2013) and Wang (2014), who identified a boundary-affected zone, specifically in areas adjacent to each sidewall with $y/W < 0.2$. (Tang et al. 2022, Wüthrich et al. 2022, 2023). For the highest Froude number, the roller toe shifted next to the sidewall implying a strong sidewall effect. The sidewall had a greater impact on the development of the shear layer compared to its effect on the upper recirculating region, discussed by Wüthrich et al. (2022) and Tang et al. (2022). The current finding further emphasised the fluctuating behaviour around $X_t(y) = x_1$ for the range $0 < y < W$. This zone appeared notably more prominent at higher Froude numbers in the present study.

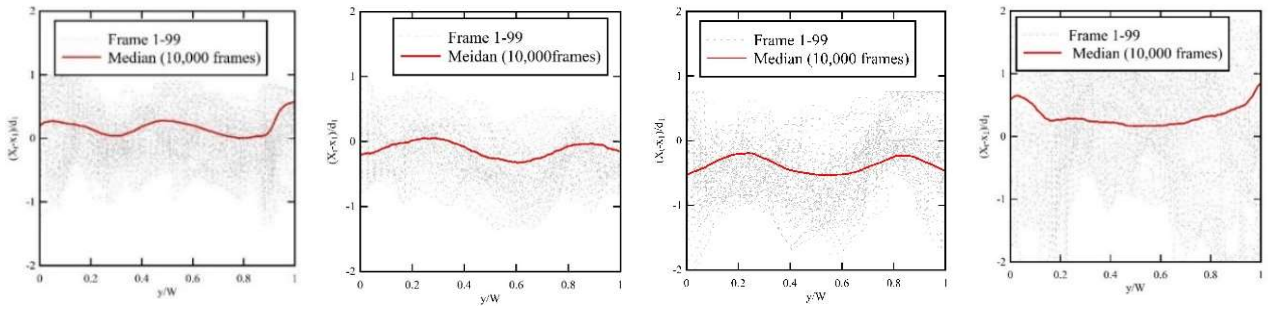

(A) (B) (C) (D)

Figure 10. Transverse distribution of the temporal median impingement perimeter of the roller front (view in elevation). Flow direction from bottom to top: (A) $Fr_1 = 2.1$; (B) $Fr_1 = 2.6$; (C) $Fr_1 = 3.1$; (D) $Fr_1 = 3.8$ - The ensemble median (red line) was calculated for 10,000 frames

5. Conclusion

The present study focused on the free-surface fluctuations and jump toe impingement characteristics in hydraulic jumps with relatively small Froude numbers ($2.1 < Fr_1 < 3.8$) and relatively large Reynolds numbers ($1.36\times10^5 < Re < 2.46\times10^5$). The visual observations showed complex transient air-water surface features, which were short-lived and very dynamic. Such air-water features included air-water packets projected above the roller and re-attaching the main flow at their impingement. The time-averaged longitudinal profile of the jump roller followed a self-similar shape, with identical results obtained with all measurement techniques. Large free surface fluctuations were recorded along the roller, with a longitudinal maximum observed in the first half of the roller. Noteworthy, the free-surface fluctuations $(d_{75}-d_{25})/d_1$ was slightly lower on the channel centreline than next to the sidewalls, likely because of the interaction between the turbulent flow and sidewalls. The roller toe perimeter was also carefully characterised. It was found that the dimensionless wave length decreased as the Froude number increased.

Acknowledgements

The authors acknowledge the technical assistance of Jason Van Der Gevel and Stewart Matthews (The University of Queensland, Australia), Jiayue Hu acknowledges the financial support of the Research Training Program (RTP), funded by the Commonwealth Government of Australia and the University of Queensland.

References

Chachereau, Y., and Chanson, H. (2011). "Bubbly Flow Measurements in Hydraulic Jumps with Small Inflow Froude Numbers." *International Journal of Multiphase Flow*, 37(6), pp. 555-564(DOI: 10.1016/j.ijmultiphaseflow.2011.03.012).

Chanson, H. (2004). "*The Hydraulics of Open Channel Flow: An Introduction*." Butterworth-Heinemann, Oxford, UK, 2nd edition, 630 pages.

Chanson, H. (2011). "Hydraulic Jumps: Turbulence and Air Bubble Entrainment." *Journal La Houille Blanche*, No. 3, pp. 5-16.

Chanson, H., and Carvalho, R. (2015). "Hydraulic Jumps and Stilling Basins" in *Energy Dissipation in Hydraulic Structures*, IAHR Monograph, CRC Press, Taylor & Francis Group, Leiden, The Netherlands, pp. 65-104.

Chanson, H., and Gualtieri, C. (2008). "Similitude and Scale Effects of Air Entrainment in Hydraulic Jumps." *Journal of Hydraulic Research*, IAHR, Vol. 46, No. 1, pp. 35-44 (DOI: 10.1080/00221686.2008.9521841) (ISSN 0022-1686).

Chow, V.T. (1959). "*Open Channel Hydraulics*." McGraw-Hill, New York, USA.

Estrella, J., Wüthrich, D., and Chanson, H. (2022). "Flow Patterns, Roller Characteristics, and Air Entrainment in Weak Hydraulic Jumps: Does Size Matter?" *Journal of Fluids Engineering*, ASME, Vol. 144, No. 7, Paper 071305, 11 pages (DOI: 10.1115/1.4053581) (ISSN 0098-2202).

Hager, W.H. (1992). "*Energy Dissipators and Hydraulic Jump.*" Kluwer Academic Publ., Water Science and Technology Library, Vol. 8, Dordrecht, The Netherlands, 288 pages.
Henderson, F.M. (1966). "*Open Channel Flow*." MacMillan Company, New York, USA.
Kucukali, S., and Chanson, H. (2008). "Turbulence Measurements in Hydraulic Jumps with Partially Developed Inflow Conditions." *Experimental Thermal and Fluid Science*, Vol. 33, No. 1, pp. 41-53 (DOI: 10.1016/j.expthermflusci.2008.06.012) (ISSN: 0894-1777).
Long, D., Rajaratnam, N., Steffler, P.M., and Smy, P.R. (1991). "Structure of flow in hydraulic jumps." *Journal of Hydraulic Research*, Vol. 29, No. 2, pp. 207–218.
Mouaze, D., Murzyn, F., and Chaplin, J.R. (2005). "Free Surface Length Scale Estimation in Hydraulic Jumps." *Journal of Fluids Engineering*, Trans. ASME, Vol. 127, pp. 1191-1193.
Murzyn, F., and Chanson, H. (2009). "Experimental investigation of bubbly flow and turbulence in hydraulic jumps." *Environmental Fluid Mechanics*, 9, pp. 143–159.
Murzyn, F., Mouaze, D., and Chaplin, J.R. (2007). "Air-Water Interface Dynamic and Free Surface Features in Hydraulic Jumps." *Journal of Hydraulic Research*, IAHR, Vol. 45, No. 5, pp. 679-685.
Novak, P., Moffat, A.I.B., Nalluri, C., and Narayanan, R. (2007). "*Hydraulic Structures*." Taylor & Francis, London, UK, 4th edition, 700 pages.
Peterka, A.J. (1958). "Hydraulic Design of Stilling Basins and Energy Dissipators." *Engineering Monograph No. 25*, United States Department of the Interior, Bureau of Reclamation, Denver, Colorado, USA, 240 pages.
Shi, R., Wüthrich, D., and Chanson, H. (2021). "Intrusive and Non-intrusive Air-water Flow Measurements in Breaking Jumps at Low Froude Number and Large Reynolds Number." *Hydraulic Model Report No. CH119/21*, School of Civil Engineering, The University of Queensland, Brisbane, Australia, 149 pages (DOI: 10.14264/4a0c07f) (ISBN: 978-1-74272-344-0).
Tang, R., Zhang, J., Bai, R., and Wang, H. (2022). "Transverse Nonuniformity of Air–Water Flow and Lateral Wall Effects in Quasi-Two-Dimensional Hydraulic Jump." *Journal of Irrigation and Drainage Engineering*, 148(10), 04022031.
Wang, H. (2014). "Turbulence and Air Entrainment in Hydraulic Jumps." *Ph.D. thesis*, School of Civil Engineering, The University of Queensland, Brisbane, Australia, 341 pages & Digital appendices (DOI: 10.14264/uql.2014.542).
Wang, H., and Chanson, H. (2015). "Air Entrainment and Turbulent Fluctuations in Hydraulic Jumps." *Urban Water Journal*, Vol. 12, No. 6, pp. 502-518 (DOI: 10.1080/1573062X.2013.847464).
Wüthrich, D., Shi, R., and Chanson, H. (2022). "Hydraulic jumps with low inflow Froude numbers: air–water surface patterns and transverse distributions of two-phase flow properties." *Environmental Fluid Mechanics*, 22(4), 789-818 (DOI: 10.1007/s10652-022-09854-5).
Wüthrich, D., Shi, R., and Chanson, H. (2023). "Discussion of 'Transverse Nonuniformity of Air–Water Flow and Lateral Wall Effects in Quasi-Two-Dimensional Hydraulic Jump.'" *Journal of Irrigation and Drainage Engineering*, 149(4), 07023004.
Zhang, G., Wang, H., and Chanson, H. (2013). "Turbulence and Aeration in Hydraulic Jumps: Free-Surface Fluctuation and Integral Turbulent Scale Measurements." *Environmental Fluid Mechanics*, 13(2), 189–204 (DOI: 10.1007/s10652-012-9254-3).